

# A Few Mode Fiber Temperature Sensor Filled With PDMS Based on Vernier Effect

Xinghu Fu<sup>1</sup>, Ran Ran, Qiannan Li, Zhexu Huang, Dongshu Li, Rongjing Zhang, Guangwei Fu<sup>2</sup>, Wa Jin, Yuefeng Qi, and Weihong Bi<sup>3</sup>

**Abstract**—A few mode fiber temperature sensor filled with PDMS based on vernier effect is proposed. It uses single mode fiber (SMF), few mode fiber (FMF), and polydimethylsiloxane (PDMS) to form the SMF-air microcavity-FMF-PDMS-FMF structure. It is to slot the glass capillary tube, place the two FMFs in the slot at a suitable distance, and fill the slot with PDMS multiple times and seal it. The PDMS is used as a sensing microcavity. We insert the SMF from the other end of the glass capillary tube, adjust the distance, fix the SMF and seal the connection. Two end faces of the SMF and the first FMF form an air reference microcavity. Since the refractive index of each medium is different, multiple reflective surfaces are formed to reflect. Because the second FMF is infinitely long, whose right end is beveled, it is considered that the sensor has four reflected beams. When the temperature changes, the length and refractive index of the PDMS microcavity will change, which will cause a change in the interference spectrum of the sensor. And because the vernier effect is formed by the superposition of the two microcavities, the temperature sensitivity can be amplified and the temperature can be measured with high sensitivity. The experimental results show that in the range of 40–56°C, the transmission spectrum of the sensor appears red shift with the increase of temperature, and the temperature sensitivity can reach 3.89nm/°C. The sensor is simple to manufacture, has high sensitivity, and has good application prospects.

**Index Terms**—Fiber optics, Vernier effect, few mode fiber, temperature.

## I. INTRODUCTION

IN RECENT years, optical fiber sensors have received great attention in people's daily life because of their compact structure, light weight, high sensitivity, fast response, and anti-electromagnetic interference [1], [2]. They have been widely used in many sensing fields, including pressure [3], [4], humidity [5], refractive index [6] and magnetic field [7], [8].

The vernier effect was originally used to improve the accuracy of length measurement. In recent years, people have tried to introduce it to improve the sensitivity of optical fiber sensors. In

order to achieve the vernier effect in the superimposed spectrum, two interferometers with similar but unequal free spectral range (FSR) must be used [9]. At present, several kinds of vernier effect fiber sensors with different sensing structures have been reported, and high-sensitivity sensing of temperature has been realized. In 2015, Shao [10] *et al.* increased the temperature sensitivity by 9 times by cascading two Sagnac interferometers. The two Sagnac interferometers use the same type of polarization maintaining fiber with slightly different lengths. The experimental results show that the temperature sensitivity can reach  $-13.36\text{nm}/^\circ\text{C}$ . In 2018, Kong [11] *et al.* designed a cylindrical fiber probe based on cascaded Fabry-Perot interferometers (FPIs). It is made by inserting single mode fiber (SMF) into a large-aperture hollow core fiber (LA-HCF) with an inner diameter of 150  $\mu\text{m}$ , and inserting the lead-in SMF into the LA-HCF from the other end. Experiments show that the sensitivity of the prepared sensor is 12.55 times higher than that of a single sensing microcavity. In 2019, Wang [12] *et al.* proposed a high-sensitivity optical fiber temperature sensor based on dual in-line Mach-Zehnder interferometers (MZI) and vernier effect. MZI is made by splicing a section of hollow-core fiber between two pieces of multimode fiber. In the range of 0–100  $^\circ\text{C}$ , the temperature sensitivity of the envelope of the superimposed spectrum reaches 528.5  $\text{pm}/^\circ\text{C}$ , which is 17.5 times of the sensor without enhancement of the vernier effect.

In the above-mentioned sensing schemes, although the sensitivity of the sensors can be greatly improved after using the vernier effect, there are still some problems. At present, common vernier effect sensors are divided into two types of structures: parallel and cascade. Parallel structures often have the shortcomings of not compact enough and complicated production process. For the cascaded vernier effect sensors, traditional all-fiber sensors often have the problem of relatively low temperature sensitivity.

This paper proposes a cascaded FPIs vernier effect temperature sensor, which uses polydimethylsiloxane (PDMS) as the heat-sensitive medium and few mode fiber (FMF) is used as the transmission medium. Due to the good thermal sensitivity of PDMS [13], the thermal sensitivity of this sensor is greatly improved compared with the traditional all-fiber F-P sensors. Compared with MMF and SMF, FMF can hold no more than ten modes. FMF sensors have more advantages in mode selection and control [14]. It has low transmission loss which attenuation coefficient is about 0.189 dB/km. And it has the advantages of low modal dispersion and low non-linearity of multimode fiber

Manuscript received August 4, 2021; revised September 7, 2021; accepted September 9, 2021. Date of publication September 14, 2021; date of current version September 27, 2021. This work was supported in part by National Natural Science Foundation of China under Grant 61735011, and in part by the S&T Program of Hebei under Grants F2021203045, 216Z1702G, 216Z1706G, and F2021203058. (Corresponding author: Xinghu Fu.)

The authors are with the School of Information Science and Engineering, The Key Laboratory for Special Fiber and Fiber Sensor of Hebei Province, Yanshan University, Qinhuangdao 066004, China (e-mail: fuxinghu@ysu.edu.cn; 710772159@qq.com; 1924972240@qq.com; 164365396@qq.com; 345071102@qq.com; 1615454827@qq.com; earl@ysu.edu.cn; jinwa@ysu.edu.cn; yfqi@ysu.edu.cn; whbi@ysu.edu.cn).

Digital Object Identifier 10.1109/JPHOT.2021.3112125

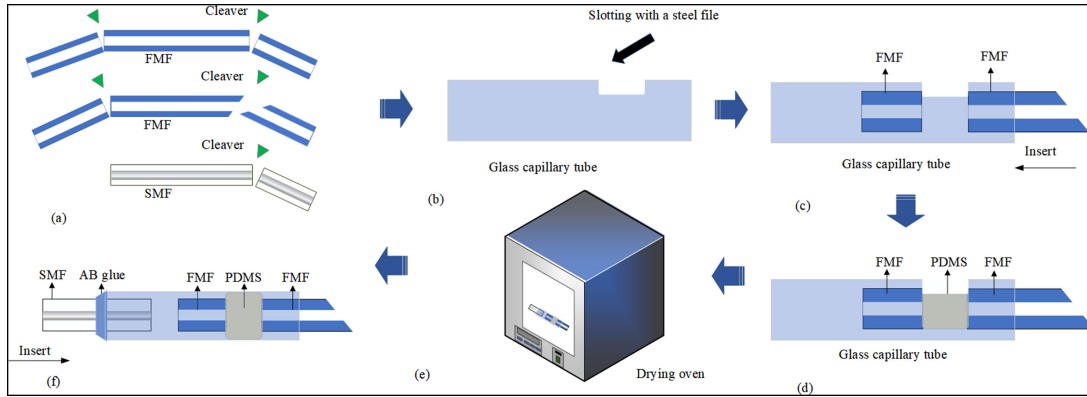


Fig. 1. The manufacturing process of the sensor: (a) cut the end of fibers (b) slot the capillary casing with a steel file (c) put the FMF in the right place (d) inject PDMS (e) heat and cure (f) place the SMF and fix the seal with AB glue.

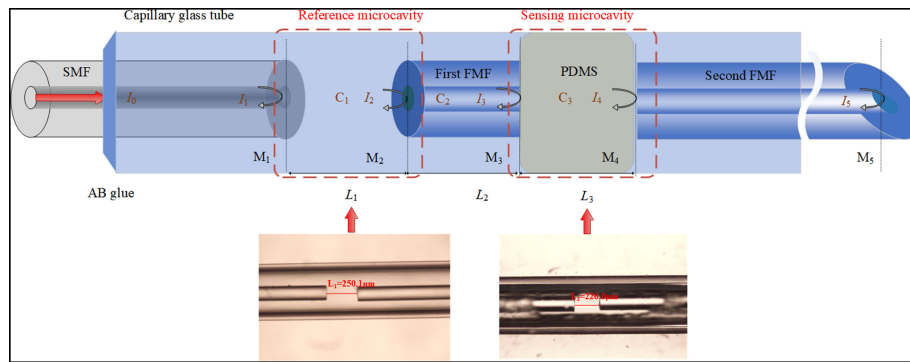


Fig. 2. Sensor structure diagram and micrograph.

[15]. The whole sensor has a compact and simple structure and its production process is simple.

## II. THE PREPARATION AND PRINCIPLE OF THE SENSOR

### A. Preparation of the Sensor

The diameter of the SMF core used in the experiment is  $9\ \mu\text{m}$ , and the cladding diameter is  $125\ \mu\text{m}$ . The FMF core diameter is  $20\ \mu\text{m}$ , and the cladding diameter is  $125\ \mu\text{m}$ . The modes that can be transmitted include LP01, LP11, LP21, and LP02. The schematic diagram of the sensor manufacturing process is shown in Fig. 1.

In Fig. 1, the manufacturing process of the sensor is as follows: First, we remove a certain length of the coating layer from the required optical fiber part and cut the end face. A steel file is used to gently scrape the surface of the glass capillary tube to slot it. In the experiment, glass fragments will inevitably fall into the tube. We first blow away the larger glass fragments, then rinse with deionized water several times to remove small fragments, and finally air-dry the glass capillary tube. Then we place the two pieces of FMF at the appropriate position, adjust the distance between the two fibers, fill the PDMS prepared with the main agent and curing agent mass ratio 10:1 at the slot, and place it in a drying oven at  $150\ ^\circ\text{C}$  for 10 minutes to cure. The PDMS microcavity can be filled and sealed by repeating the injection and heating process multiple times. The purpose of filling the PDMS multiple times is to make the PDMS in the microcavity

more uniform. Before filling, the configured liquid PDMS is allowed to stand for about three minutes to eliminate air bubbles by gravity. We ensure that the filling of PDMS is slow, which can effectively avoid the generation of bubbles. Finally, we insert the SMF, adjust its position so that the length of the air microcavity is at an appropriate length, then use AB glue to fix and seal it.

### B. Sensing Principle

The structure of the few mode fiber temperature sensor based on PDMS filling and vernier effect is shown in Fig. 2. So we fabricated a cascaded FPIs sensor whose  $L_1$ ,  $L_2$ , and  $L_3$  are  $250.1\ \mu\text{m}$ ,  $15\ \text{mm}$ , and  $226.0\ \mu\text{m}$  respectively. The photomicrographs of the reference microcavity and sensing microcavity of the prepared sensor are shown in the illustrations.

It can be seen from Fig. 2 that due to the different refractive index of fibers, air, and PDMS, five reflective surfaces are formed, corresponding to  $M_1$ ,  $M_2$ ,  $M_3$ ,  $M_4$ , and  $M_5$ . The light emitted by the light source propagates forward from the core of the SMF, the input light intensity is set to  $I_0$ , and the reflected beam intensity is set to  $I_1$ ,  $I_2$ ,  $I_3$ ,  $I_4$ , and  $I_5$ . Since the length of the second FMF is very long, about  $150\ \text{mm}$ , and the right fiber end face is beveled, the light intensity  $I_5$  is relatively small and can be ignored. And because the first FMF with a length of  $15\ \text{mm}$  is used as a transmission fiber, it is much longer than the length of the two microcavities, so the reflection spectrum is more concise, which can be regarded as the spectrum formed

by the cascade of two FPIs, and the total intensity of the final reflection back to the SMF can be simplified as [16]:

$$I = I_1 + I_2 + I_3 + I_4 + 2\sqrt{I_1 I_2} \cos\left(\frac{4\pi n_1 L_1}{\lambda}\right) + 2\sqrt{I_3 I_4} \cos\left(\frac{4\pi n_3 L_3}{\lambda}\right) \quad (1)$$

where  $n_1$  and  $n_3$  are the refractive index of the air microcavity  $C_1$  and the PDMS microcavity  $C_3$  respectively, and the corresponding lengths of the two microcavities are  $L_1$  and  $L_3$  respectively.  $\lambda$  is the wavelength of incident light.

When the temperature changes, due to the good thermal performance of PDMS, the microcavity length and refractive index will change significantly. At room temperature, the refractive index is 1.399, the thermal expansion coefficient can reach  $9.6 \times 10^{-4}/^\circ\text{C}$ , and the thermo-optic coefficient is  $-5.0 \times 10^{-4}/^\circ\text{C}$ . Therefore, the microcavity  $C_3$  serves as a sensing microcavity in the vernier effect. In contrast, the thermal performance of air is relatively stable, and the microcavity  $C_1$  is air-tight, and the air pressure in the microcavity further guarantees the stability of the microcavity, so  $C_1$  is used as the reference microcavity. The free spectral range (FSR) of the reference microcavity and the sensing microcavity is defined as

$$\begin{cases} FSR_r = \frac{\lambda^2}{2n_1 L_1} \\ FSR_s = \frac{\lambda^2}{2n_3 L_3} \end{cases} \quad (2)$$

The two microcavities are cascaded and a curve with an envelope will be observed. The FSR of the envelope curve is

$$FSR_{envelope} = M \cdot FSR_s \quad (3)$$

where  $M$  is the sensitivity magnification of the spectral envelope after cascading relative to the sensing sensitivity of a single sensing microcavity. The value of  $M$  is

$$M = \frac{FSR_r}{|FSR_r - FSR_s|} \quad (4)$$

Therefore, when the temperature changes, the sensitivity of the envelope can be amplified by a large magnification relative to the temperature sensitivity of a single sensing microcavity.

When the reference microcavity length  $L_1$  of the sensor is  $250 \mu\text{m}$  and the sensing microcavity length  $L_3$  is  $226 \mu\text{m}$ , the simulated interference spectrum is shown in Fig. 3.

It can be seen from Fig. 3 that under the condition of  $40^\circ\text{C}$ , the single sensing microcavity will red shift about  $0.86 \text{ nm}$  when the temperature rises by  $1^\circ\text{C}$ . Under the same conditions, the cascade-FPIs structure has a red shift of about  $4.10 \text{ nm}$ , and the sensitivity is increased by about 4.77 times. Substituting the relevant parameters into (2) for calculation, it can be concluded that the FSR of the reference microcavity and the sensing microcavity are  $4.81 \text{ nm}$  and  $3.80 \text{ nm}$ , respectively. Substituting the two FSR calculation results into (4) for calculation, we can obtain that the magnification ratio is 4.76. The result basically agrees with the calculated result.

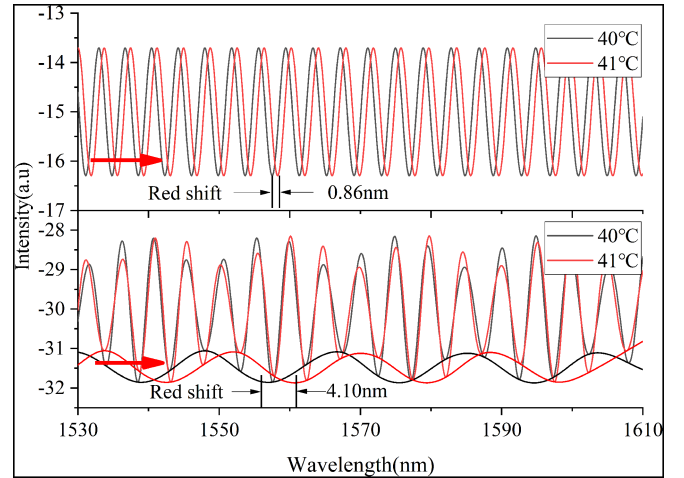


Fig. 3. Simulated interference spectroscopy (a) single microcavity (b) cascaded FPIs.

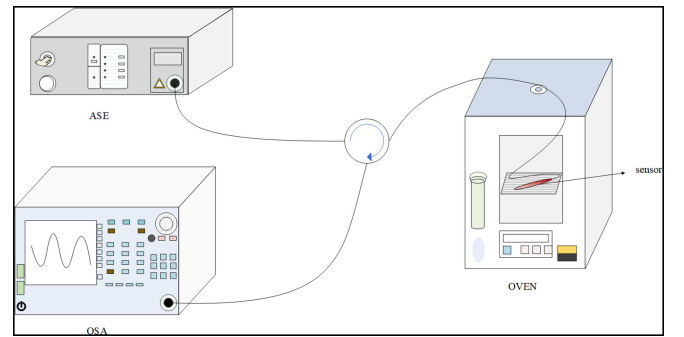


Fig. 4. Schematic diagram of the experimental system.

### III. EXPERIMENTS AND ANALYSIS

#### A. Temperature Experiment

The experimental device for testing the temperature characteristics of the sensor is shown in Fig. 4. It consists of a broadband light source (ASE, wavelength range of  $1520\text{--}1610 \text{ nm}$ , output power  $50\text{mW}$ ), optical spectrum analyzer (OSA, AQ6375), optical circulator (OC, center wavelength of  $1550\text{nm}$ ) and a temperature control box (WHL-30B, resolution of  $0.1^\circ\text{C}$ ).

As shown in Fig. 4, the light emitted by the light source passes through the OC to reach the sensor, and the reflected light passes through the OC to reach the OSA. The temperature range is from  $40^\circ\text{C}$  to  $56^\circ\text{C}$ . Due to the high sensitivity of the sensor, the wavelength will shift about  $3.89 \text{ nm}$  for every  $1^\circ\text{C}$  increase. In  $1520\text{--}1610 \text{ nm}$ , when the temperature changes too much, the marked peak will shift out of this wavelength detection range and it also will not show on the spectrum, so the tested temperature range is relatively tiny. The temperature rise step length is chosen to be  $1^\circ\text{C}$ . The spectrum and its envelope at  $40^\circ\text{C}$  are shown in Fig. 5.

We fit the envelope curve of the spectrum, and compare the envelope shift at different temperatures. The experimental results are shown in Fig. 6.

It can be seen from Fig. 6 that during the heating process of  $40\text{--}56^\circ\text{C}$ , the envelope curve has obvious red shift. The

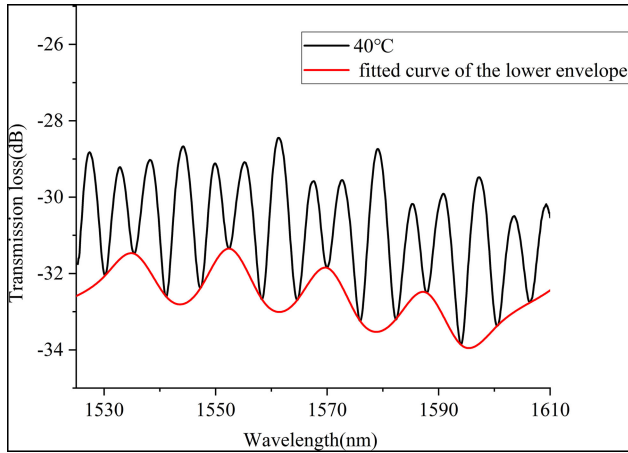


Fig. 5. Sensor spectrum at 40 °C.

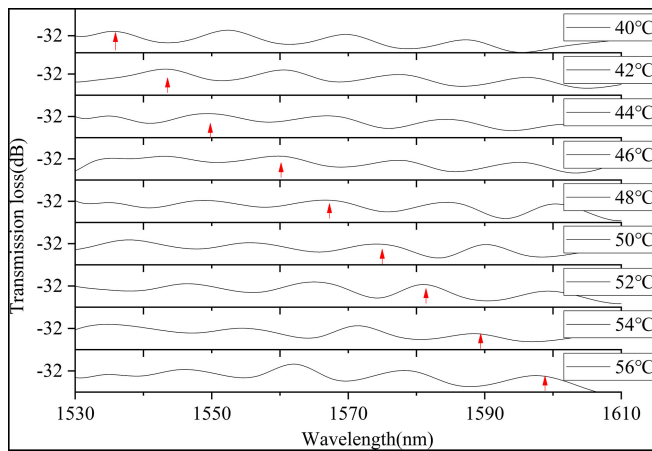


Fig. 6. Envelope drift diagram.

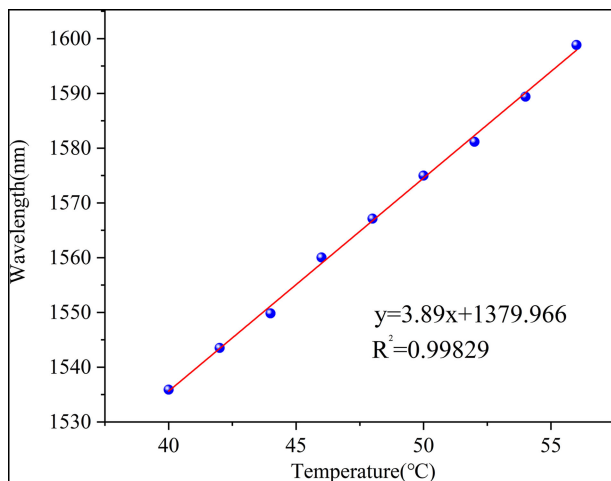


Fig. 7. Linear fitting diagram.

spectral envelopes at different temperatures are calibrated with red arrows on the peaks, and the wavelengths are linearly fitted to the corresponding temperatures. The fitting diagram obtained is shown in Fig. 7.

In Fig. 7, it can be concluded that the sensor sensitivity can reach 3.89nm/°C in the range of 40–56 °C, which is basically

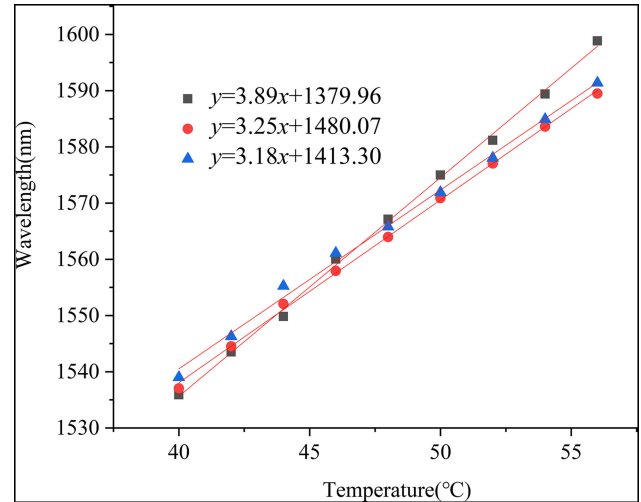


Fig. 8. Repeatability experiment.

TABLE I  
COMPARISON OF SENSOR PERFORMANCE WITH DIFFERENT STRUCTURES

Sensor structure	Sensitivity	Temperature range
Cascade of Sagnac interferometers <sup>[10]</sup>	-13.36 nm/°C	30–40°C
Cascade of FPIs <sup>[11]</sup>	-1.081 nm/°C	30–42°C
Parallel In-Line MZIs <sup>[12]</sup>	528.5 pm/°C	0–100°C
This paper	3.98nm/°C	40–56°C

consistent with the simulation result. However, due to certain errors in the measurement environment, there will be slight differences between the experimental results and the simulation results.

### B. Repeatability Experiment

In order to check the stability of the sensor, repeated measurements were performed 24 hours and 48 hours after the first experiment, and the results were compared. The linear fitting diagram of the experimental results is shown in Fig. 8.

It can be seen that the sensitivity of the sensor also changes slightly as time changes. It has good repeatability and stability. The sensitivity of the sensor has slightly decreased in the three experiments, and the reasons for this situation may include: a certain error in the measurement, and the thermal expansion of the sensing medium is slightly reduced caused by the repeated experiments.

We compared the sensor proposed in this article with the sensors proposed in other documents, and the comparison results are shown in Table I.

Although the cascaded Sagnac sensor [10] has high temperature sensitivity, its temperature measurement range is small and its structure is not compact enough. Cascaded FPIs sensor [11] use the thermal expansion of silicon to achieve sensing, so the sensitivity is low. Similarly, the parallel in-line MZIs sensor [12] also has the same problem, and the sensor is a parallel structure,



which is more complicated. In contrast, the sensor proposed in this paper has the advantages of high sensitivity, simple structure, and easy fabrication.

#### IV. CONCLUSION

This paper presents a few mode fiber temperature sensor based on PDMS filling and vernier effect. The air microcavity and PDMS are used as the reference microcavity and the sensing microcavity to realize the vernier effect. The sensing principle of the sensor is analyzed, and the relationship between temperature and spectrum is simulated. In this paper, temperature experiments are performed on the sensor, and the lengths of the reference microcavity and the sensing microcavity are 250 $\mu\text{m}$  and 226 $\mu\text{m}$ , respectively. The experimental results show that the temperature sensitivity of the sensor is 3.98nm/ $^{\circ}\text{C}$  in the temperature range of 40–56  $^{\circ}\text{C}$ , and there is a good linear relationship between wavelength shift and temperature change. The sensor has high sensitivity, simple manufacture, compact structure, and high practicability.

#### REFERENCES

- [1] M. Q. Chen *et al.*, “High sensitivity temperature sensor based on fiber air-microbubble Fabry–Perot interferometer with PDMS-filled hollow-core fiber,” *Sensors Actuators A: Phys.*, vol. 275, pp. 60–66, Jun. 2018.
- [2] J. K. Peng *et al.*, “Dielectric film based optical fiber sensor using Fabry–Perot resonant structure,” *Opt. Commun.*, vol. 430, pp. 63–67, Jan. 2019.
- [3] Y. Zhao, M. Q. Chen, R. Q. Lv, and F. Xia, “In-fiber rectangular air fabry-perot strain sensor based on high-precision fiber cutting platform,” *Opt. Commun.*, vol. 384, pp. 107–110, Feb. 2017.
- [4] P. Xia *et al.*, “A High-temperature resistant photonic crystal fiber sensor with single-side sliding Fabry–Perot cavity for super-large strain measurement,” *Sensors Actuators A: Phys.*, vol. 318, Feb. 2021, Art. no. 112492.
- [5] C. Zhou *et al.*, “High-sensitivity relative humidity fiber-optic sensor based on an internal–external Fabry–Perot cavity Vernier effect,” *Opt. Exp.*, vol. 29, no. 8, pp. 11854–11868, Apr. 2021.
- [6] X. H. Fu *et al.*, “Simultaneous measurement of temperature and refractive index with F–P microcavity sensor based on graded-index few mode fiber,” *Opt. Commun.*, vol. 455, Jan. 2020, Art. no. 124577.
- [7] Q. Liu, L. Xing, and Z. X. Wu, “The highly sensitive magnetic field sensor based on photonic crystal fiber filled with nano-magnetic fluid,” *Opt. Commun.*, vol. 452, pp. 238–246, Dec. 2019.
- [8] Y. Dong *et al.*, “Magnetic field and temperature sensor based on D-shaped fiber modal interferometer and magnetic fluid,” *Opt. Laser Technol.*, vol. 107, pp. 169–173, Nov. 2018.
- [9] T. J. Yao, S. L. Pu, Y. L. Zhao, and Y. Q. Li, “Ultrasensitive refractive index sensor based on parallel-connected dual Fabry–Perot interferometers with Vernier effect,” *Sensors Actuators A: Phys.*, vol. 290, pp. 14–19, May 2019.
- [10] L. Y. Shao *et al.*, “Sensitivity-enhanced temperature sensor with cascaded fiber optic Sagnac interferometers based on Vernier effect,” *Opt. Commun.*, vol. 336, pp. 73–76, Feb. 2015.
- [11] L. X. Kong *et al.*, “Cylinder-type fiber-optic Vernier probe based on cascaded Fabry–Perot interferometers with a controlled FSR ratio,” *Appl. Opt.*, vol. 57, no. 18, pp. 5043–5047, Jun. 2018.
- [12] Z. R. Wang, L. Huang, C. Liu, H. Wang, S. Sun, and D. Yang, “Sensitivity-Enhanced fiber temperature sensor based on Vernier effect and dual in-line Mach–Zehnder interferometers,” *IEEE Sensors J.*, vol. 19, no. 18, pp. 7983–7987, Sep. 2019.
- [13] J. Li *et al.*, “Microfiber Fabry–Perot interferometer used as a temperature sensor and an optical modulator,” *Opt. Laser Technol.*, vol. 129, Sep. 2020, Art. no. 106296.
- [14] X. H. Fu *et al.*, “A multi-directional magnetic field sensor based on tapered few mode fiber and magnetic fluid,” *Optik*, vol. 240, Aug. 2021, Art. no. 166817.
- [15] F. Ren *et al.*, “Design of weakly-coupled eccentric-ring core few-mode fiber for optical sensing,” *Opt. Commun.*, vol. 490, Jul. 2021, Art. no. 126924.
- [16] J. J. Tian, Z. G. Li, Y. X. Sun, and Y. Yao, “High-sensitivity Fiber–Optic strain sensor based on the vernier effect and separated Fabry–Perot interferometers,” *J. Lightw. Technol.*, vol. 37, no. 21, pp. 5609–5618, Nov. 2019.